# Static Modulation Wave of Halogen-Bond Network Transduced to a Hierarchy of Change Stimuli of Crystalline Rotors Dynamics

Sergey Simonov,<sup>1,2</sup> Leokadiya Zorina,<sup>1,2</sup> Pawel Wzietek,\*3 Antonio Rodríguez-Fortea,<sup>4</sup> Enric Canadell,\*5 Cécile Mézière,<sup>1</sup> Guillaume Bastien,<sup>1</sup> Cyprien Lemouchi,<sup>1</sup> Miguel Garcia-Garibay,\*6 and Patrick Batail\*1

## Affiliations:

<sup>1</sup>Laboratoire MOLTECH-Anjou, CNRS UMR 6200, Université d'Angers, France <sup>2</sup>Institute of Solid State Physics, Russian Academy of Sciences, Chernogolovka MD, Russia <sup>3</sup>Laboratoire de Physique des Solides, CNRS UMR 6502, Université de Paris-Sud, Orsay, France <sup>4</sup>Departament de Química Física i Inorgànica, Universitat Rovira i Virgili, Marcel·li Domingo 1, 43007 Tarragona, Spain

<sup>5</sup>Institut de Ciència de Materials de Barcelona (ICMAB-CSIC), Campus de la UAB, 08193 Bellaterra, Spain

<sup>6</sup>Department of Chemistry, University of California—Los Angeles, United States

email addresses of corresponding authors <u>pawel.wzietek@u-psud.fr</u>, <u>canadell@icmab.es</u>, mgg@chem.ucla.edu, and patrick.batail@univ-angers.fr

**Abstract**: Here we present a study where what can be seen as a static modulation wave across halogen-bond arrays of crystalline 1,4-Bis((4'-(iodoethynyl)phenyl)ethynyl) bicyclo[2,2,2]octane rotors changes the structure from one-half molecule to three-and-a-half molecules in the asymmetric unit below a phase transition at 105 K. The remarkable finding is that the most complex total  ${}^{1}H$  spin-lattice relaxation rate,  $T_{1}^{-1}$ , revealed to date in molecular rotors is the weighted sum of the relaxation rates of the four contributing rotors relaxation rates, each with distinguishable exchange frequencies reflecting Arrhenius parameters with different activation barriers (Ea) and attempt frequencies ( $\tau_0$ ). This allows us to show, in tandem with rotor-environment interaction energy calculations, how the dynamics of molecular rotors are able to decode structural information from their surroundings with remarkable precision.

Just as it is essential to biological phenomena, for example the growth or turning movement of an organism, usually a plant, tend to respond in a complex but reliable manner when subject to subtle environmental stimuli, understanding such events is important in the realms of materials chemistry and physics of molecular machines because the development of elaborate sensory devices is also required to accurately report changes that occur in the environment of their dynamic components. [2-5,7-9]

Here we present a study where what can be seen as a static modulation wave across 1,4-Bis((4'-(iodoethynyl)phenyl)ethynyl) halogen-bond arrays<sup>[6,7]</sup> crystalline of bicyclo[2,2,2]octane rotors, 1 (Figure 1) changes the structure from one-half molecule to three-and-a-half molecules in the asymmetric unit below a phase transition at 105 K. The remarkable finding is that the complex, total <sup>1</sup>H spin-lattice relaxation rate,  $T_1$ -1, revealed by variable-temperature, variable-field experiments is the weighted sum of the relaxation rates of the four contributing rotors relaxation rates. Hence, magnetic relaxation transforms from a process determined by a single molecular rotator in the high temperature phase into one that has distinguishable weighted contribution from the four new sites, each with distinguishable exchange frequencies reflecting Arrhenius parameters with different activation barriers (Ea) and attempt frequencies ( $\tau_0$ ). This allows us to show, in tandem with rotor-environment interaction energy calculations, how the dynamics of molecular rotors are able to decode structural information from their surroundings with remarkable precision.

$$F = \begin{cases} F \\ F \\ F \end{cases}$$

$$F = \begin{cases} F \\ F \\ F \end{cases}$$

$$F = \begin{cases} F \\ F \\ F \end{cases}$$

$$F = \begin{cases} F \\ F \\ F \end{cases}$$

$$F = \begin{cases} F \\ F \\ F \end{cases}$$

$$F = \begin{cases} F \\ F \\ F \end{cases}$$

$$F = \begin{cases} F \\ F \\ F \end{cases}$$

$$F = \begin{cases} F \\ F \\ F \end{cases}$$

$$F = \begin{cases} F \\ F \\ F \end{cases}$$

$$F = \begin{cases} F \\ F \\ F \end{cases}$$

$$F = \begin{cases} F \\ F \\ F \end{cases}$$

$$F = \begin{cases} F \\ F \\ F \end{cases}$$

$$F = \begin{cases} F \\ F \\ F \end{cases}$$

$$F = \begin{cases} F \\ F \\ F \end{cases}$$

$$F = \begin{cases} F \\ F \\ F \end{cases}$$

$$F = \begin{cases} F \\ F \\ F \end{cases}$$

$$F = \begin{cases} F \\ F \\ F \end{cases}$$

$$F = \begin{cases} F \\ F \\ F \end{cases}$$

$$F = \begin{cases} F \\ F \\ F \end{cases}$$

$$F = \begin{cases} F \\ F \\ F \end{cases}$$

$$F = \begin{cases} F \\ F \\ F \end{cases}$$

$$F = \begin{cases} F \\ F \\ F \end{cases}$$

$$F = \begin{cases} F \\ F \\ F \end{cases}$$

$$F = \begin{cases} F \\ F \\ F \end{cases}$$

$$F = \begin{cases} F \\ F \\ F \end{cases}$$

$$F = \begin{cases} F \\ F \\ F \end{cases}$$

$$F = \begin{cases} F \\ F \\ F \end{cases}$$

$$F = \begin{cases} F \\ F \\ F \end{cases}$$

$$F = \begin{cases} F \\ F \\ F \end{cases}$$

$$F = \begin{cases} F \\ F \\ F \end{cases}$$

$$F = \begin{cases} F \\ F \\ F \end{cases}$$

$$F = \begin{cases} F \\ F \\ F \end{cases}$$

$$F = \begin{cases} F \\ F \\ F \end{cases}$$

$$F = \begin{cases} F \\ F \\ F \end{cases}$$

$$F = \begin{cases} F \\ F \\ F \end{cases}$$

$$F = \begin{cases} F \\ F \\ F \end{cases}$$

$$F = \begin{cases} F \\ F \\ F \end{cases}$$

$$F = \begin{cases} F \\ F \\ F \end{cases}$$

$$F = \begin{cases} F \\ F \\ F \end{cases}$$

$$F = \begin{cases} F \\ F \\ F \end{cases}$$

$$F = \begin{cases} F \\ F \\ F \end{cases}$$

$$F = \begin{cases} F \\ F \\ F \end{cases}$$

$$F = \begin{cases} F \\ F \\ F \end{cases}$$

$$F = \begin{cases} F \\ F \\ F \end{cases}$$

$$F = \begin{cases} F \\ F \\ F \end{cases}$$

$$F = \begin{cases} F \\ F \\ F \end{cases}$$

$$F = \begin{cases} F \\ F \\ F \end{cases}$$

$$F = \begin{cases} F \\ F \\ F \end{cases}$$

$$F = \begin{cases} F \\ F \\ F \end{cases}$$

$$F = \begin{cases} F \end{cases}$$

$$F = \begin{cases} F \\ F \end{cases}$$

$$F = \begin{cases} F \end{cases}$$

$$F = \begin{cases} F \\ F \end{cases}$$

$$F = \begin{cases} F \end{cases}$$

$$F = \begin{cases} F \\ F \end{cases}$$

$$F = \begin{cases} F \end{cases}$$

$$F = F \end{cases}$$

$$F = \begin{cases} F \end{cases}$$

$$F = \begin{cases} F \end{cases}$$

$$F = \begin{cases}$$

**Figure 1**. Structure of molecular rotor **1**. Together with  $2^{[7b]}$  and 1,4-bis(iodoethynyl)bicyclo[2.2.2]octane (BIBCO)<sup>[7a]</sup> they are a class of halogen-bonded, self-assembled crystalline rotors. Both **2** and BIBCO were previously shown to display ambient temperature dynamics in the GHz regime. Preparation and characterization of compound **1** are described in the Supporting Information section.

A set of three halogen-bonding interactions serves to direct the self-assembly of two-dimensional arrays of  $\bf 1$  (Figure 2). While  $\delta_1$  and  $\delta_2$  are common to  $\bf 1$  and BIBCO (Figure S1), we show here that the installation of ethynylphenyl fragments on the BIBCO frame provides additional molecular degrees of freedom that, expressed through C-I··· $\pi$  interaction  $\delta_3$ , [10] confers a unique collective behavior to the dynamics of  $\bf 1$ .

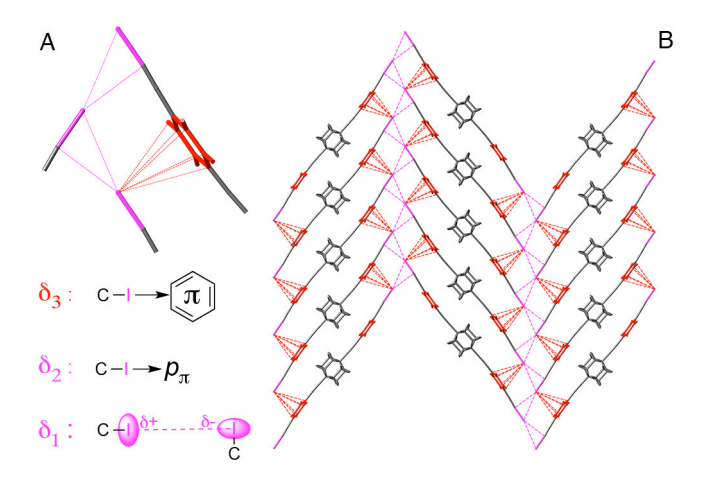


*Figure 2*. (A) The three types of halogen-bonds and their schematic representations. (B) A single two-dimensional array self-assembled out of  $\delta_1$ ,  $\delta_2$  and  $\delta_3$  in the structure of **1** at 120 K. Note that only one out of the two equilibrium rotator positions are depicted here.

We have observed that the monoclinic unit cell of a single crystal of 1 abruptly changes, experiencing below 105 K (Figure 3B) a dramatic expansion by seven times its volume to encompass three and a half independent rotators at 90 K, labeled I to IV in Figure 3C (only one-half independent rotor in the asymmetric unit is present in the structure of 1 at 120 K; details of the investigation of the reversible transition and structure refinements at 120 K, Figure 3A, and 90 K, Figure 3C, can be found in the Supporting Information and Figures S4-S5, S7-S8). It is even more remarkable that the layer-by-layer packing has each of the four halogen-bonded homogenous arrays of independent rotators stacked in alternating sequences, color-coded red (I), gold (II), blue (III) and black (IV) in Figure 3C. Moreover, the layers are stacked in registry yet alternately sliding by one-half molecular length. Thus, the inter-layer interactions primarily involve C-H···I hydrogen bonds (Figure 3A and 3C) that define four distinct rotor-environment pockets. The origin of the differentiation of these pockets lies in what is seen as a static modulation wave of all three  $\delta_1$ ,  $\delta_2$  and  $\delta_3$  halogen bonds encompassing the four homogenous layers of independent rotators I, II, III and IV, typically adjusting the degree of freedom of the  $\delta_3$ -bond manifold. For example, note that all phenyl rings are parallel at 120 K; then see in Figure S8 the distribution of dihedral angles between two phenyl rings at 90 K, from 0° in IV, to 25.6°, 14.7° and 3.1° in I. II and III. respectively. Moreover, the single C-I···I-C halogen bond, δ<sub>1</sub> (I...I, 4.049 Å) at 120 K bursts at the transition into seven different bonds with I...I distances in the range of 3.885-4.334 Å.

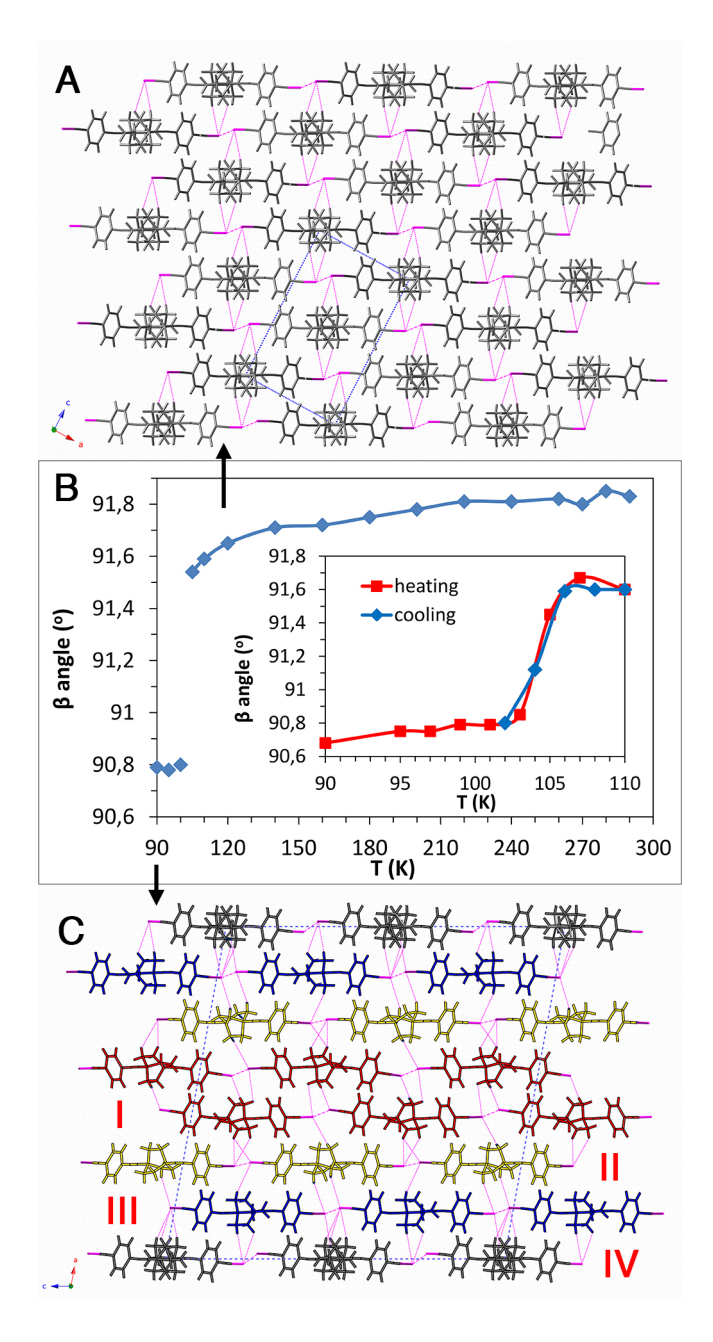


**Figure 3**. (A) Layer-by-layer packing of arrays of the single one-half independent rotators (disordered with balanced occupancies on two equilibrium positions) in the structure of  $\bf 1$  at 120 K. Dotted red lines are  $\delta_1$  interactions and C–H···I hydrogen bonds by which the rotators rub on their environment. (B) The reversible structure transition (see also Figures S4-S6) illustrated by an abrupt change of the monoclinic angle  $\beta$ . (C) Below the transition, a static modulation wave of the three halogen-bonding interactions encompasses a registry of four different arrays (I to IV) shown here at 90 K. Note that only one rotator (IV) is disordered with balanced occupancies while all three other independent rotators have one equilibrium position only.

Variable-field  $^{1}$ H and  $^{13}$ C solid state NMR experiments carried out on static crystalline samples over large temperature and pressure windows have illuminated our understanding of the balance of competing electronic instabilities coupled to molecular degrees of freedom at the heart of the rich quantum physics in low dimension in strongly correlated molecular conductors.  $^{[11]}$  Translating to the realm of molecular rotors the ability to perform variable-field, variable-temperature proton spin-lattice relaxation time experiments,  $^{1}$ H  $^{-1}$ , has recently demonstrated great promise to gain insight into the dynamics of crystalline rotors and help disentangle multiple relaxation processes eventually occurring all at once at the same spin temperature (see the basic principles in the Supporting Information).  $^{[7,8,9]}$  Here, variable-temperature (20–300 K) proton spin-lattice relaxation experiments carried out at two  $^{1}$ H Larmor frequencies on a polycrystalline sample of 1 reveal at the temperature of the structural transition a reversible discontinuity (Figure 4) similar to that occurring in 2,  $^{[7b]}$  another extended analog of BIBCO also endowed with the additional degree of freedom conferred by two phenyl rings implemented in the rod axle (Figure 1).

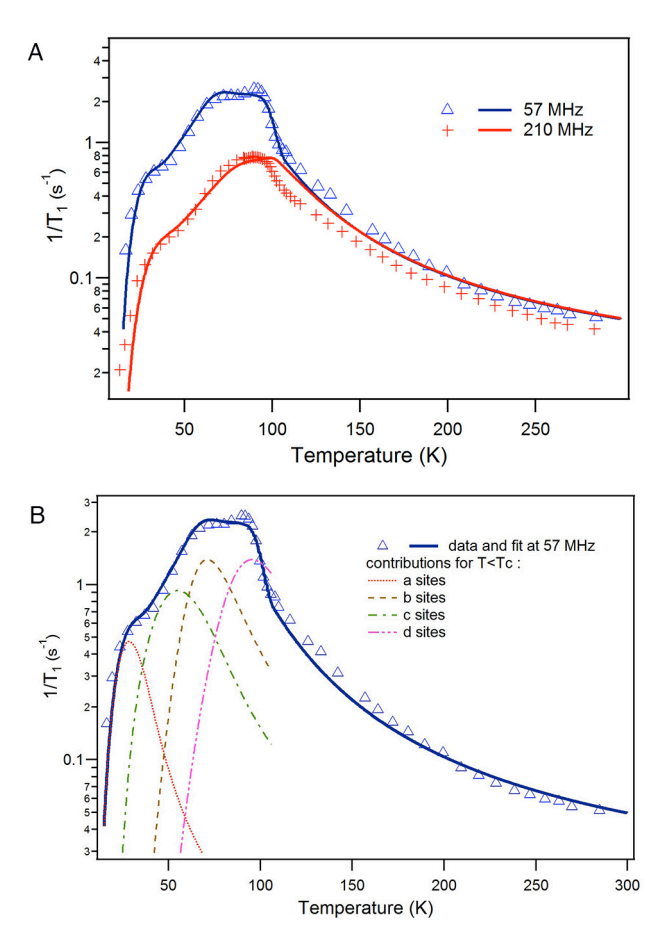


**Figure 4**. (A) Variable-temperature <sup>1</sup>H spin-lattice relaxation time  $T_1^{-1}$  at 57 and 210 MHz for **1**. The blue and red lines represent the fits<sup>[12]</sup> of the data to a sum of standard Kubo-Tomita expressions, with thermally activated correlation times  $\tau_i = \tau_0 \exp(E_i/kT)$  where  $E_i$  denotes the energy barrier at site i (see text and Supporting Information). (B) Curves for each of the four components of the total relaxation ( $T < T_c$ ) drawn for one frequency.

Below the phase transition, the  $T_1^{-1}$  data display several entangled maxima; this is not unexpected since the analysis of the structure at 90 K led us to explicit an inventory of a total of four independent rotator sites that would result in complex dynamics encompassing as many independent relaxation processes. The intensity of  $T_1^{-1}$  maxima scales with the net number of moving <sup>1</sup>H on each independent site; hence, the fits of the data to the Kubo-Tomita (KT) formula for  $T_1$  with correlation times  $\tau_i = \tau_0 \exp(E_i/kT)$  were conducted with the knowledge that, below the transition, rotators I, II and III each involves 2/7 of the total number of moving protons, rotators IV having 1/7 of the net number. Therefore, the low temperature data can be fitted with a weighted sum of four KT expressions with different energy barriers (Figure 4B and Supporting Information), hereafter noted  $E_a$ ,  $E_b$ ,  $E_c$ ,  $E_{IV}$ . Note that the first three barriers refer to rotators I, II and III and cannot be assigned solely from the fits because they have the same weight. On the other hand, all moving protons are located on a single independent site at 120 K, therefore above the transition temperature,  $T_{\rm c}$ , the fit was done assuming a single barrier, noted  $E_{\rm HT}$ . To simplify the fits, all processes were assigned a common attempt frequency,  $\tau_0$ ; this is expected for identical rotors since  $\tau_0$ is a frequency characteristic of a specific, freely moving rotor. The best fit shown in Figure 4A was obtained with  $\tau_0 = 1.8 \times 10^{-12} \text{ s.}$ 

For T>T<sub>c</sub> , the fit yields  $E_{\rm HT}$  = 429 K (0.85 kcal mol<sup>-1</sup>). For the low temperature phase, we could not obtain good fits with fixed barriers, which let us to assume the existence of a slight disorder implying a distribution of energy barriers. A Gaussian distribution was then set for each barrier, with the  $\sigma$  values of their respective relative widths given below in percent of the barrier values. Likewise, we assumed a slight distribution of the transition temperature Tc in the fit. The fits shown in Figure 4 yield  $E_{\rm IV}$  = 188 K (0.37 kcal mol<sup>-1</sup>),  $\sigma_{\rm IV}$  = 20%,  $E_a$  = 486 K (0.97 kcal mol<sup>-1</sup>),  $\sigma_a$  = 1.2%,  $E_b$  =360 K (0.72 kcal mol<sup>-1</sup>),  $\sigma_b$  = 22%,  $E_c$  = 651 K (1.29 kcal mol<sup>-1</sup>),  $\sigma_c$  = 1.9%, Tc = 100 K,  $\sigma_{Tc}$  = 3.6% (Table S2).

Assigning relaxation processes at the nano- and micro-scale, be they discrete events on distinct sites<sup>[7a,b,8a,c]</sup> or dual, coupled processes associated with correlated rotational motion in well-separated pairs of rotators,<sup>[8b,9]</sup> requires the fits to the  $T_1^{-1}$  data to be coupled to calculations<sup>[7b,8-9]</sup> of rotor-environment interaction energies (Table S2). At this point, assigning the experimental barrier above the transition as well as that of rotor IV is non-ambiguous; therefore, we are left to match barriers  $E_a$ ,  $E_b$  and  $E_c$  with rotators in arrays I, II, and III. Thus, we have estimated the five rotational barriers (Figure 5) for each independent rotator by means of partial geometry optimizations (rotor itself and the nearest molecules of the environment interacting with it through I atoms) using the same computational details reported previously.<sup>[7b]</sup>

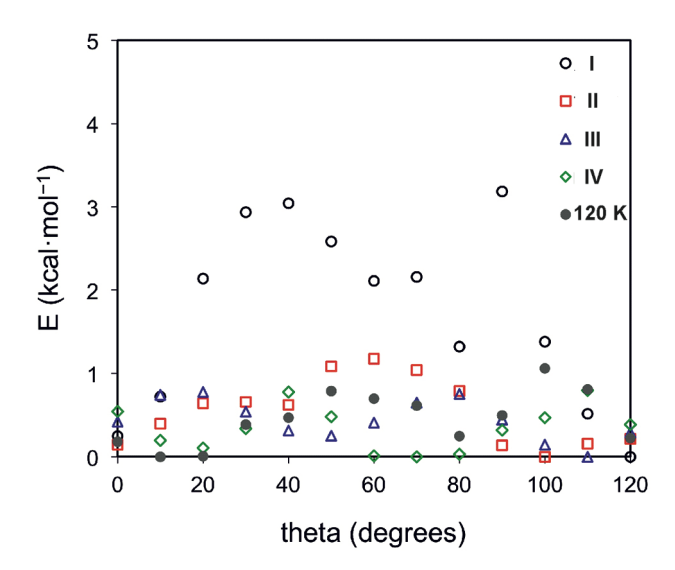


*Figure 5*. Computed energy profiles (in kcal mol<sup>-1</sup>) for the rotation of each independent rotator surrounded by their neighbor molecules; the five models for the DFT transition structures are described in Figure S11.

All barriers (Figure 5 and Figure S11) are calculated around 1 kcal mol<sup>-1</sup> (0.78-1.18) except that for rotator I in the 90 K structure which is noticeably higher at 3.19 kcal mol<sup>-1</sup> (1605 K). This is because shorter H···I contacts occur in the transition state for I, including a contact as short as 2.94 Å. In contrast, rotators in sites II, III and IV have no contact shorter than 3.2 Å when the geometry of their transition structures is optimized along their rotational trajectories. For example, the shorter H···I contact for II, the 120 K rotator, and IV are 3.20-3.21 Å; they are even larger, 3.276 Å for III. Therefore, the activation barriers seem to be primarily determined by the strength of the shorter H···I contacts in their transition state.

Moreover, the values of the calculated barriers listed in Figure 5 allow for the assignment (Table S2 and Figure S11) of the rotational barriers extracted from the fits of the  $T_1^{-1}$  data between 20 K and 300 K; both are fully coherent and qualify a global rotor dynamics characterized by one large rotational barrier supplemented by two pairs of smaller ones separated by  $\sim 124$  K (proton spin-lattice experiments) or  $\sim 166$  K (rotor-environment energy calculations). The remarkable agreement demonstrated here testifies the validity of this integrated approach.

Beyond the nanoscale change stimuli of the present crystalline rotor dynamics, providing information on their surroundings with a remarkable level of accuracy, other concerted changes are hidden in rich phase diagrams to be disclosed by opening large temperature windows, integrating structure, spin-lattice relaxation, dielectric and second-order nonlinear optical experiments, and rotor-environment energy calculations. Unraveling the phase diagrams of these materials, also tackling in future work their response to uniaxial and isostatic pressure, is interesting because they could be used as simulators to control molecular machines.

In addition to drawing attention to the susceptibility of extended, non-covalent halogen-bond arrays to undergo concerted modulation in their temperature phase

diagram,<sup>[7a,b]</sup> the results observed with compound  $\mathbf{1}$  provide<sup>[7a,b,8,9]</sup> the kind of in-depth insight on the mechanism of motion required on the way towards a control of molecular machines.<sup>[2-5]</sup>

# Supporting Information

Supporting Figures and Tables, Synthesis, Crystal structures at 120 K and 90 K, VT <sup>1</sup>H spinlattice relaxation time: basic principles and experimental details, computational details. CCDC 1577087 contains the crystallographic data for this paper. These data can be obtained free of charge from The Cambridge Crystallographic Data Centre.

# **Acknowledgments**

This research was funded by the CNRS, the University of Angers, the University of Paris-Sud, Orsay; the Région des Pays de la Loire Grant MOVAMOL, the joint CNRS-Russian Federation grants PICS 6028 and RFBR-CNRS 12-03-91059 (Chernogolovka). Work at UCLA was supported by USA National Science Foundation grants DMR140268 and DMR-1700471. Work in Bellaterra and Tarragona was supported by the Spanish Ministerio de Economía y Competitividad (Grants FIS2015-64886-C5-4-P and CTQ2014-52774-P) and Generalitat de Catalunya (2014SGR301 and 2014SGR199). E.C. acknowledges support by MINECO (Spain) through the Severo Ochoa Centers of Excellence Program (Grant SEV-2015-0496). S.S.; C. L. and G. B.; thank the CNRS and the Région des Pays de la Loire for a post-doctoral and Ph. D. grants, respectively. L. Z. thanks the CNRS for an Associated Researcher Fellowship.

## **Conflict of interest**

The authors declare no conflict of interest.

**Keywords**: molecular rotors  $\cdot$  proton spin-lattice relaxation time  $\cdot$  mechanism of motion  $\cdot$  phase transition  $\cdot$  self-assembly  $\cdot$  halogen bonding  $\cdot$  supramolecular chemistry

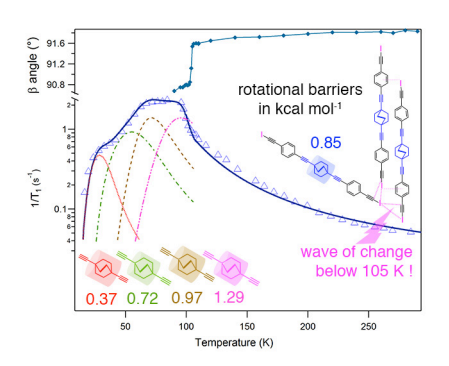
#### References

- [1] (a) L. S. Kocsis, K. M. Elbel, M. A. Hardigree, K. M. Brummond, M. A. Haidekker, E. A. Theodorakis, *Org. Biomol. Chem.* **2015**, *13*, 2965; and reference 1 therein. (b) B. G. Pickard, *Current Topics in Membranes* **2007**, *58*, 361; DOI: 10.1016/S1063-5823(06)5814-7.
- [2] J. A. Abendroth, O. S. Bushuyev, P. S. Weiss, C. J. Barrett, ACS Nano 2015, 9, 7746.
- [3] S. Erbas-Cakmak, D. A. Leigh, C. T. McTernan, A. L. Nussbaumer, *Chem. Rev.* **2015**, *115*, 10081. DOI: 10.1021/acs.chemrev.5b00146
- [4] S. R. Domingos, A. Cnossen, W. J. Buma, W. R. Browne, B. L. Feringa, M. Schnell, *Angew. Chem. Int. Ed.* **2017**, *56*, 11209. DOI: 10.1002/anie.201704221
- [5] C. S. Vogelsberg, M. A. Garcia-Garibay, *Chem. Soc. Rev.* **2012**, *41*, 1892.
- [6] Selected references on halogen bonding: (a) A. C. Legon, *Phys. Chem. Chem. Phys.* **2010**, *12*, 7736. (b) M. Fourmigué, *Curr. Opinion Sol. St. Mater. Sc.* **2009**, *13*, 36. (c) R. Bertani, P. Sgarbossa, A. Venzo, F. Lelj, M. Amati, G. Resnati, T. Pilati, P. Metrangolo, G. Terraneo, *Coord. Chem. Rev.* **2012**, *254*, 677. (d) R. W. Troff, T. Mäkelä, F. Topic, A. Valkonen, K. Raatikainen, K. Rissanen, *Eur. J. Org. Chem.* **2013**, 1617. (e) F. Meyer, P. Dubois, *CrystEngComm* **2013**, *15*, 3058.

- [7] Halogen-bonding in crystalline rotors: (a) C. Lemouchi, C. Vogelsberg, S. Simonov, L. Zorina, P. Batail, S. Brown, M. Garcia-Garibay, *J. Am. Chem. Soc.* **2011**, *133*, 6371. (b) C. Lemouchi, H. M. Yamamoto, R. Kato, S. Simonov, L. Zorina, A. Rodríguez-Fortea, E. Canadell, P. Wzietek, I. Iliopoulos, D. Gindre, M. Chrysos, P. Batail, P. *Cryst. Growth Des.* **2014**, *14*, 3375. (c) L. Catalano, S. Perez-Estrada, G. Terraneo, T. Pilati, G. Resnati, P. Metrangolo, M. A. Garcia-Garibay, *J. Am. Chem. Soc.* **2015**, *137*, 18386. (d) L. Catalano, S. Perez-Estrada, H.-H. Wang, A. J.-L. Ayitou, S. I. Khan, G. Terraneo, P. Metrangolo, S. Brown, M. A. Garcia-Garibay, *J. Am. Chem. Soc.* **2017**, *139*, 843.
- [8] (a) C. Lemouchi, C. Mézière, L. Zorina, S. Simonov, A. Rodríguez-Fortea, E. Canadell, P. Wzietek, P. Auban-Senzier, C. Pasquier, T. Giamarchi, M. A. Garcia-Garibay, P. Batail, J. Am. Chem. Soc. 2012, 134, 7880. (b) C. Lemouchi, K. Iliopoulos, L. Zorina, S. Simonov, P. Wzietek, T. Cauchy, A. Rodríguez-Fortea, E. Canadell, J. Kaleta, J. Michl, D. Gindre, M. Chrysos, P. Batail, J. Am. Chem. Soc. 2013, 135, 9366. (c) G. Bastien, C. Lemouchi, P. Wzietek, S. Simonov, L. Zorina, A. Rodríguez-Fortea, E. Canadell, P. Batail, Zeit. Anorg. Allg. Chem. 2014, 640, 1127-1133.
- [9] (a) G. Bastien, C. Lemouchi, M. Allain, P. Wzietek, A. Rodríguez-Fortea, E. Canadell, K. Iliopoulos, D. Gindre, M. Chrysos, P. Batail, *CrystEngComm* 2014, 16, 1241. (b) J. Kaleta, J. Michl, C. Mézière, S. Simonov, L. Zorina, P. Wzietek, A. Rodríguez-Fortea, E. Canadell, P. Batail, *CrystEngComm* 2015, 17, 7829.
- [10] J. Cao, X. Yan, W. He, X. Li, Y. Mo, M. Liu, T.-B. Jiang, J. Am. Chem. Soc. **2017**, 139, 6605.
- [11] See, for example: (a) L. Zorina, S. Simonov, C. Mézière, E. Canadell, S. Suh, S. E. Brown, P. Foury-Leylekian, P. Fertey, J. P. Pouget, P. Batail, *J. Mater. Chem.* 2009, 19, 6980-6994. (b) S. A. Baudron, P. Batail, C. Coulon, R. Clérac, E. Canadell, V. Laukhin, R. Melzi, P. Wzietek, D. Jerome, P. Auban-Senzier, S. Ravy, *J. Am. Chem. Soc.* 2005, 127, 11785-11797. (c) K. Miyagawa, K. Kanoda, A. Kawamoto, *Chem. Rev.* 2004, 104, 5635-5653. (d) S. Lefebvre, P. Wzietek, S. Brown, C. Bourbonnais, D. Jérome, C. Mézière, M. Fourmigué, P. Batail, *Phys. Rev. Lett.* 2000, 85, 5420-5423. (e) H. Mayaffre, P. Wzietek, C. Lenoir, D. Jérome, P. Batail, *Europhys. Lett.* 1994, 28, 205-210.
- [12] Multi-parameter fits of the NMR relaxation were done using a genetic optimisation algorithm; see for example: (a) M. Wormington, C. Panaccione, K. M. Matney, D. K. Bowen, *Phil. Trans. R. Soc. Lond. A* **1999**, *357*, 2827-2848. (b) A. Nelson, *J. Appl. Cryst.* **2006**, *39*, 273.

S. Simonov, L. Zorina, P. Wzietek,\* A. Rodríguez-Fortea, E. Canadell,\* C. Mézière, G. Bastien, C. Lemouchi, M. Garcia-Garibay,\* P. Batail\*

Static Modulation Wave of Halogen-Bond Network Transduced to a Hierarchy of Change Stimuli of Crystalline Rotors Dynamics



**Wave of change**: A static modulation at 105 K across parallel halogen-bonded arrays results in four, instead of one, distinct crystallographic bicyclo[2.2.2]octane rotator sites. The remarkable finding is that the complex, total  $^1\mathrm{H}$  spin-lattice relaxation rate,  $T_1^{-1}$ , is the weighted sum of the relaxation rates of the four contributing rotors relaxation rates, allowing, in tandem with rotor-environment interaction energy calculations, to decode structural information from their surroundings with remarkable precision.